ACS OMEGA

Open Access

http://pubs.acs.org/journal/acsodf

Article

Silica-Reinforced AMP−Calcium Alginate Beads for Efficient and Selective Removal of Cesium from a Strong Acidic Medium

Qiang Jin, Xinya Diao, Ye Fan, Lecun Hao, Zongyuan Chen, and Zhijun Guo*

Cite This: *ACS Omega* 2024, 9, 32011−32020

Read Online

ACCESS | Metrics & More | Article Recommendations

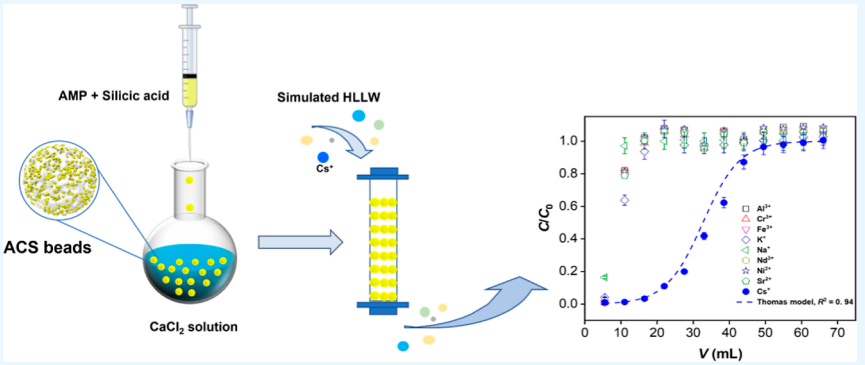

ABSTRACT: Due to the significant selectivity for Cs^+, ammonium molybdophosphate (AMP) possesses potential to uptake radiocesium from high-level liquid waste (HLLW), whereas its micro-crystalline structure and fine powder morphology limit its industrial application. Although the granulation method with alginate is prospective for the preparation of an AMP exchanger, the mechanical strength of obtained beads may be insufficient for application. In this context, we prepared silica-reinforced AMP−calcium alginate (ACS) beads and evaluated their performance for Cs^+ removal from strong acidic solutions. It was found that the addition of silica in the fabrication significantly improved the mechanical strength of the beads in comparison to those without silica. Notably, the beads with an AMP/silica mass ratio of 1.0 exhibited an exceptional mechanical strength, surpassing that of ACS beads composed of other components. The batch experiment results indicated that the Cs^+ adsorption follows a non-linear pseudo-second-order rate equation. The distribution coefficient of Cs^+ was high even in extreme acidic conditions (~1.6×10^2 mL/g in 8.0 mol/L HNO_3 solution). The Cs^+ adsorption can be well fitted with the Langmuir model, and the estimated maximum exchange capacity in 3.0 mol/L HNO_3 could reach 23.9 mg/g. More importantly, ACS beads showed excellent selectivity toward Cs^+ uptake over eight co-existing metal ions in simulated HLLW, with separation factor values all above 145. The column experiment exhibited that the beads can serve as the stationary phase in columns to effectively remove Cs^+. The findings of this study are significant as they provide insights into the development of efficient materials for radiocesium removal from high-level liquid waste. The results demonstrate the potential of silica-reinforced ACS beads for Cs^+ adsorption, with promising applications in industrial settings.

1. INTRODUCTION

How to treat radioactive wastewater efficiently has become the most critical issue in the development of nuclear energy technology. High yield fission products ^{135}Cs and ^{137}Cs are present in the acidic high-level liquid waste (HLLW).[1] ^{135}Cs (half-life = 2.3×10^6 years) is a long-lived radionuclide that can cause a harmful effect on the environment after its discharge from the repository along with other radioisotopes. In contrast, ^{137}Cs (half-life = 30.1 years) is one of heat generators in HLLW and its removal leads to the reduction in heat load, and hence, the lower volume of repository is needed for final vitrification. Also, ^{137}Cs, being a β,γ-emitter, is extensively utilized in medical, industrial, and agricultural fields.[2−4] Therefore, the efficient removal and capture of radiocesium from HLLW is crucial for reducing disposal costs, protecting the environment, and promoting resource recycling.

Due to the high acidic and high-salinity nature of the HLLW, the efficient capture of radiocesium from HLLW still remains to be a challenging task. Various separation techniques,[5] including chemical precipitation, liquid−liquid extraction, and ion exchange/adsorption, have been utilized to

Received: April 21, 2024
Revised: June 20, 2024
Accepted: July 1, 2024
Published: July 12, 2024

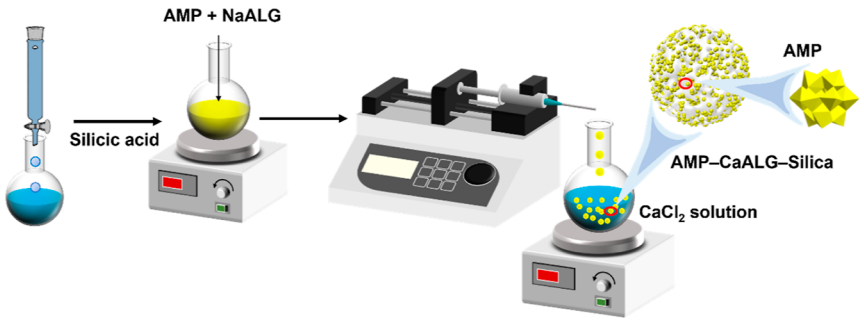

Figure 1. Fabrication process of the composite. In the figure, some images are sourced from https://mp.weixin.qq.com/s/_jBXVGvgJa8OCSHgGDxUoQ and free domain.

enrich and separate radiocesium. These methods, however, have certain drawbacks in terms of operating conditions, cost, productivity, stability, or selectivity, such as the large amount of radioactive sludge generated by precipitation and the costly and hazardous extractants employed in solvent extraction techniques.[6] The ion exchange method may overcome the disadvantages mentioned above,[7] whereas the method requires the development of highly efficient ion exchangers with high capacity and selectivity for Cs^+ in acidic solutions.

Ammonium molybdophosphate (AMP), $[(NH_4)_3P\text{-}(Mo_3O_{10})_4]$, a kind of heteropoly acid salt, has been recognized as one of the most promising adsorbents for separation of Cs^+ due to the unique Keggin structure.[8] The NH_4^+ associated in the gap of the $[P(Mo_3O_{10})_4]^{3-}$ spherical anion can exchange with Cs^+ with high specificity, and the crystalline structure of AMP remains remarkably stable even in strongly acidic conditions.[9] However, due to its microcrystalline structure and undesirable hydraulic characteristic, AMP cannot be directly used as the stationary phase in columns,[10] impeding its industrial application.

Preparation of AMP-based adsorbents into granular form remains challenge. Alginate, a popular natural polymer, has attracted wide interest for immobilization purposes of powder-type adsorbents due to its ability to form three-dimensional gelled beads when exposed to divalent cations such as Ca^{2+}.[11] The granulation with alginate gel has several advantages such as low cost, simplicity for preparation, and strong acid resistance.[12] However, in real-time operation, the Ca^{2+} cross-linked alginate beads are readily swollen and ruptured.[13] From an engineering materials perspective, organic−inorganic hybrid materials have the potential to overcome the limitations of alginate as a binding polymer.[14] Among the various inorganic components that have been hybridized with alginate, silica has attracted considerable attention.[15−18] Silica produced by the condensation of their silanol surface groups can form a tighter interface with polymer matrices in hybrid materials and provide polymer scaffolds with the ability to biomineralize, increasing the mechanical, thermal, and stiffness properties of the material.[18] Encapsulating enzymes and cells within the alginate/silica composite has been widely studied in the biomedical field.[17,18] This provides important guidance for the potential application of alginate/silica composite to immobilize Cs^+ adsorbent.

Herein, we synthesized a new silica-functionalized AMP−calcium alginate (ACS) beads through the sol−gel method. The effectiveness of the obtained beads in removing Cs^+ from strongly acidic solutions was subsequently assessed with batch and column experiments. As a composite material composed of AMP, calcium alginate, and silica, its synthesis should be optimized first to obtain a highly efficient adsorbent with high mechanical strength and excellent ion exchange capacity. In addition, the current siliceous composite materials are generally prepared from organic precursors such as tetraethyl orthosilicate and tetramethyl orthosilicate $Si(OMe)_4$ (TMOS).[19] However, inorganic silicates like sodium/potassium silicates and liquid glass are more economic and environmental-friendly than organic precursors. Therefore, in this study, we opted to use the cheap and easily available sodium silicate to produce the silica component. The objectives of this study were to (1) optimize the mass ratio of AMP to silica within composite; (2) investigate the influence of contact time, HNO_3 concentration, initial Cs^+ concentration, and coexisting ions on the adsorption process; (3) analyze the adsorption behavior of Cs^+ on the basis of kinetic and isothermal adsorption models as well as XPS characterization; and (4) assess the potential of the beads for Cs^+ uptake in practical application. The research results are highly significant for the removal of radioactive Cs^+ from HLLW.

2. EXPERIMENTAL SECTION

2.1. Chemicals. All reagents were commercialized and used without further purification. AMP (CAS: 54723-94-3) and sodium alginate (NaALG) were purchased from Macklin company. Sodium silicate (sodium metasilicate pentahydrate, $Na_2SiO_3{\cdot}5H_2O$) was obtained from Tianjin Balance Bio-Tech Co, Ltd. 732-type strong acid cation exchange resin was purchased from Shandong Chemical Co. Other reagents were obtained from Tianjin Guangfu Fine Chemical Industry Research Institute. Aqueous solutions were prepared using distilled water with a resistivity of 18.2 $M\Omega{\cdot}cm^{-1}$ obtained from a Millipore water purification system. For security, non-radioactivity $^{133}CsNO_3$, supplied by Shanghai Tianlian Chemical Technology Co., Ltd., was used in this work. A stock solution of 7.52×10^{-3} mol/L Cs^+ was prepared by dissolving $CsNO_3$ in distilled water. Caution: the emission of β- and γ-particles from ^{135}Cs to ^{137}Cs poses a significant health risk. Hence, experiments involving these radioisotopes should be conducted in a radiation laboratory equipped with HEPA filtered hoods, gloveboxes, and continuous air monitors.

2.2. Preparation of Spherical Composite Adsorbent. The synthesis of a spherical composite adsorbent is schematically shown in Figure 1. In a typical experiment, 7.07 g of $Na_2SiO_3{\cdot}5H_2O$ (containing 2.00 g SiO_2) was dissolved in 20.0 mL of distilled water and the solution was passed through a column of 732-type strong acid cation exchange resin

https://doi.org/10.1021/acsomega.4c03806
ACS Omega 2024, 9, 32011−32020

according to the well-established procedure to obtain a silicic acid solution.[20] The silicic acid solution was subsequently mixed with 0.80 g of NaALG and different amounts of AMP (0.40, 2.00, 5.00, and 10.0 g). At the moment, the corresponding mass ratios of AMP to silica in mixed solutions were 0.2:1, 1:1, 2.5:1, and 5:1, respectively. After stirring for 4 h, the uniform mixture was added dropwise into a 0.1 mol/L $CaCl_2$ solution using an automatic syringe with a 0.7 mm-diameter needle and stirred to form the beads. The injection speed was controlled at 20−30 drops/min, while maintaining a distance of 5−10 cm between the needle and the $CaCl_2$ solution. The obtained gelled beads were furtherly reinforced by aging for an additional 24 h. Finally, the prepared beads were separated by filtration, washed with distilled water several times, and air-dried at 50 °C for 6 h before used. The spherical composite adsorbents prepared by beads of AMP/CaALG with silica are termed as ACS-*X*, where *X* denotes the mass ratio of AMP/silica in the composite (e.g., ACS-1.0 represents an ACS with the mass ratio of AMP to silica of 1.0). For comparison, AMP−CaALG composite was prepared by a similar process without adding silicic acid.

2.3. Characterization. X-ray diffraction (XRD) pattern measurements of samples were carried out using an X-ray diffractometer (X'Pert Pro, PANalytical) equipped with Cu Kα radiation (λ = 1.54178 Å) and a scanning range of 5−70°. The functional groups present in the ACS beads were investigated using Fourier transform infrared (FT-IR) spectra. The spectra were recorded from 400 to 4000 cm^{-1} with an accumulation of 16 scans (iS50, Nicolet). The morphology surfaces were characterized by scanning electron microscopy (SEM, Apreo S, Thermo Fisher Scientific) at 15 kV. Further qualitative elemental compositional investigation at the selected spots of sample surface was performed via energy-dispersive spectroscopy (EDS), using an Oxford Instruments X-MaxN EDS detector. N_2 adsorption and desorption isotherm at 77 K was employed to determine pore textural properties including the specific Brunauer−Emmett−Teller (BET) surface area and micropore volume by using a N_2 adsorption apparatus (ASAP 2020M, Micromeritics). The mechanical strength measurement was performed using a particle strength tester (KDZ-1, Shandong Yuntang intelligent Technology Co., Ltd., China). Five replicates of each specimen were measured and the average value was taken. XPS measurements were performed using an ESCALab220i-XL surface microanalysis system (VG Scientific) equipped with Al Kα ($h\nu$ = 1486.6 eV) and a chamber pressure of 3×10^{-9} mbar. The C 1s peak of 284.4 eV was used as a reference.

2.4. Batch Adsorption−Desorption Experiment. Batch-type adsorption experiments were carried out in an acidic solution to verify the feasibility of the adsorbent for removing Cs^+ in HLLW. For each experiment, a total of 20.0 mg of adsorbent and 2.0 mL of HNO_3 solution (0.1−8.0 mol/L) containing the Cs^+ were mixed in a polyethylene tube. Then, the mixture was shaken mechanically at 400 rpm for a certain contact time to achieve equilibrium state. After that, the two phases were separated by filtration using a 0.22 μm Millipore syringe filter. The effect of parameters including contact time, HNO_3 concentration, initial Cs^+ concentration, and interfering metals in the simulated HLLW on Cs^+ adsorption was explored. After adsorption, the Cs^+ loaded adsorbents were eluted using an NH_4NO_3 solution to evaluate the desorption ability of adsorbent.

The concentrations of metal ions were determined by an inductively coupled plasma optical emission spectrometer (ICP−OES, PQ9000, Analytik Jena GmbH). The adsorption percentage (%), adsorption capacity (q, mg/g), distribution coefficient (K_d, mL/g), and the separate factors (SF) of Cs^+ from interfering metals are defined as

$$\text{adsorption}\ (\%) = \frac{C_0 - C_t}{C_0} \times 100\% \quad (1)$$

$$q = (C_0 - C_t)\frac{V}{m} \quad (2)$$

$$K_d = \frac{C_0 - C_t}{C_0}\frac{V}{m} \quad (3)$$

$$SF = \frac{K_{d,Cs}}{K_{d,M}} \quad (4)$$

where C_0 and C_t (mol/L) represent the concentration metal ions before adsorption and adsorbed at time t (h), V (L) the volume of aqueous solution, m (g) the mass of the adsorbent, and M represents different metallic ions. All the experimental data were the average of duplicate or triplicate experiments and the relative error was less than 5%.

2.5. Column Experiment. Dynamic adsorption experiments were performed in a polyvinyl chloride column with an internal diameter of 0.96 cm and a height of 4.0 cm. The vertically oriented column was uniformly wet-packed with 1.00 g of granulated adsorbent. The Cs^+ solution was passed through the column at a flow rate of 0.55 mL/min, which was controlled via a peristaltic pump. Effluent was collected at 5.50 mL intervals and the Cs^+ concentration was measured by ICP−OES. The breakthrough curve was expressed as relative concentration (C/C_0) versus effluent volume, where C (mol/L) and C_0 (mol/L) were concentrations of Cs^+ in the effluents and influents, respectively.

3. RESULTS AND DISCUSSION

3.1. Preparation and Characterization of Encapsulated Adsorbents. The granulated ACS composite was synthesized by a simple sol−gel method owing to the network confined effect of silica−alginate hybrid hydrogels. In this work, the ACS beads were prepared with a mass ratio of AMP to silica ranging from 0.2 to 5.0. It is well-known that the higher AMP content within composite seems to afford more exchange sites for the Cs^+ removal. However, by increasing the AMP loading content, the lower mechanical strength for ACS beads was observed. As shown in Figure 2, the mechanical strength of ACS beads increased from 20.6 to 68.8 N $particle^{-1}$ with the increasing of AMP/silica mass ratio from 0.4 to 1.0, whereas, at higher AMP/silica mass ratio, the mechanical strength was decreased. Therefore, synthesizes mechanical strength and ion exchange capacity, granulated ACS composite with AMP/silica mass ratio of 1.0 (i.e., ACS-1.0) were relatively and preferentially selected as an exchanger on Cs^+ uptake from aqueous solution in the subsequent experiment. Note that, as expected, the mechanical strength of ACS-1.0 beads are significantly higher than that of AMP−CaALG composite (24.8 N·$particle^{-1}$) without incorporation of amorphous silica. This is in good agreement with the literature,[15−18] i.e., the presence of silica could strength the alginate matrix' mechanical resistance.

https://doi.org/10.1021/acsomega.4c03806
ACS Omega 2024, 9, 32011−32020

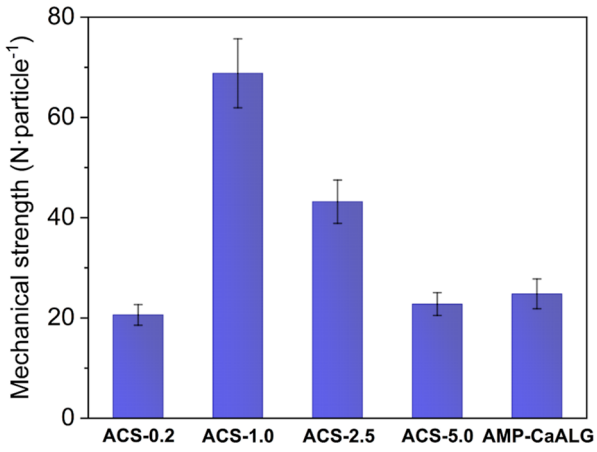

Figure 2. Mechanical strengths of ACS beads with different AMP/silica mass ratios.

According to Figure 3a,b, the prepared ACS-1.0 beads were well-defined at the diameter size of 1.5 mm after the whole procedure, which is beneficial to minimize the pressure drop loss during the column experiment.[9] On the surface of the obtained beads, some cracks were observed and a number of fine AMP crystals were seen to be encapsulated (Figure 3c). EDS analysis (Figure 3d) revealed the dispersion of C, Ca, P, Cl, N, Mo, and Si elements within the composite.

FT-IR analyses were conducted to determine the functional groups present in the hybrid material. In Figure 4a, a distinct band at 3446 cm^{-1} was attributed to O−H stretching of interlayer water molecules as well as layer hydroxyl groups, and IR frequencies at 2923, 1636, and 1404/3220 cm^{-1} corresponded to the presence of $-CH_2$ (blending), −COO− (symmetric and asymmetric stretching), and N−H (blending) in the ACS-1.0 beads.[21] The band at 451 cm^{-1} is attributed to the Si−O group.[13] Furthermore, four vibrational bands at 1064, 961, 869, and 790 cm^{-1} are indicative of P−O, Mo−O, and Mo−O−Mo groups, which can be attributed to the intact Keggin structure of $[PMo_{12}O_{40}]^{3-}$.[22]

The XRD patterns of pure AMP powder and ACS-1.0 beads are shown in Figure 4b, in which peak profiles of the composite are attributed to the excellent crystallinity of AMP. However, CaALG and silica, both of which have amorphous structures,[23,24] do not exhibit distinct diffraction peaks in the XRD patterns. Pure AMP shows some strong peaks at 10.4, 15.1, 18.3, 21.5, 24.3, 26.5, 30.4, 36.2, and 55.4° (2θ), and these diffraction peaks are indexed as the (110), (200), (211), (220), (310), (222), (400), (332), and (550) reflections associated with the Keggin structure.[25] The results corresponded to the FT-IR analyses (Figure 4a).

The properties of the composite material were furtherly characterized by N_2 adsorption−desorption isotherms, which are shown along with pore-size distributions in Figure 4c,d. The plots of ACS-1.0 beads can be classified a typical type-IV pattern with an H3-type hysteresis loop according to International Union of Pure and Applied Chemistry classifications.[26] The BET surface area and pore volume of the beads were thus determined to be 84.64 m^2/g and 0.036 cm^3/g, respectively.

3.2. Kinetic Study. A batch experiment was conducted to determine the optimal time required to achieve adsorption equilibrium for Cs^+ uptake. According to Figure 5, it was found that the ACS-1.0 beads are highly effective in rapidly adsorbing Cs^+ ions under acidic conditions. The uptake of Cs^+ in a 3.0 mol/L HNO_3 solution is initially fast, reaching equilibrium within 12 h. This can be attributed the abundance of available adsorption sites of AMP within the composite, resulting in a high adsorption rate. However, as the contact time progresses, the adsorption process slows down due to a decrease in the number of available adsorption sites. The ACS-1.0 beads removal kinetics are comparable with some AMP-based composites including the AMP/PVA/SA composite (equili-

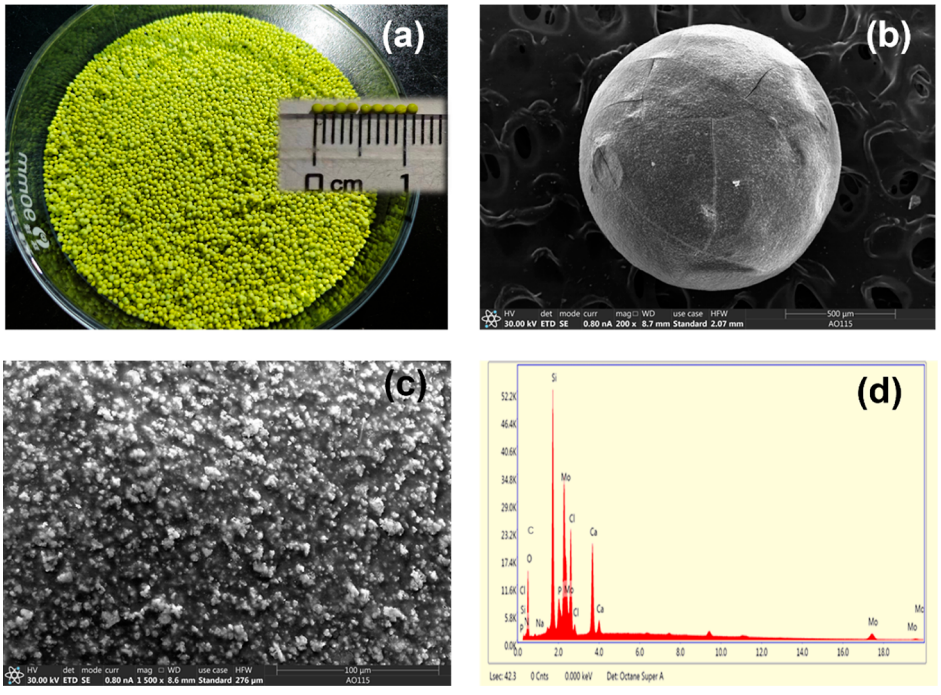

Figure 3. Photographic image (a), SEM images (b,c), and the corresponding EDX analysis (d) of the synthesized adsorbent.

https://doi.org/10.1021/acsomega.4c03806
ACS Omega 2024, 9, 32011−32020

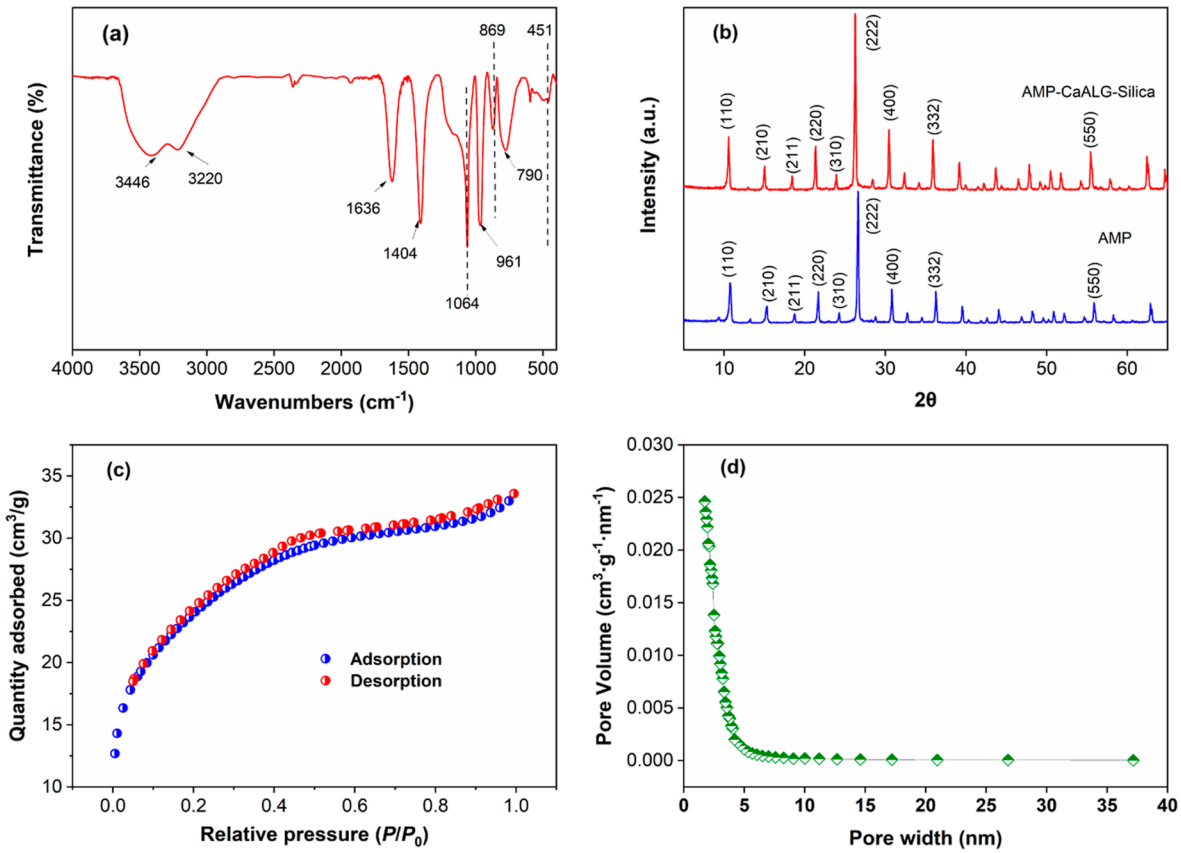

Figure 4. XRD pattern (a), FT-IR spectra (b), N_2 adsorption−desorption isotherms, (c) and corresponding pore-size distribution curve (d) of ACS-1.0 beads.

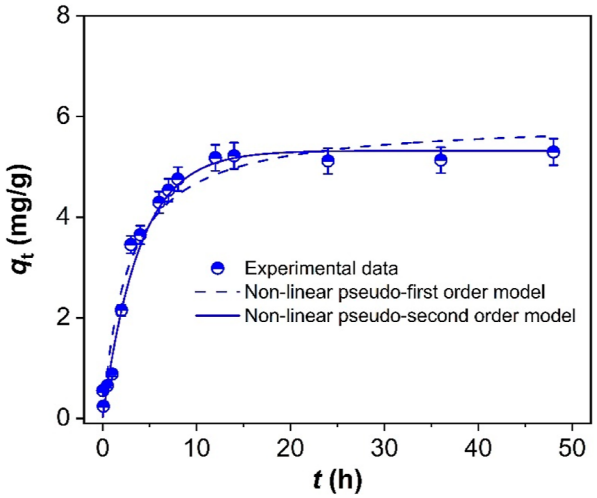

Figure 5. Kinetics of Cs^+ removal by ACS-1.0 beads. $[Cs^+]$ = 3.75 × 10^{-4} mol/L, m/V = 10 g/L, and $[HNO_3]$ = 3.0 mol/L.

brium time, t_e = 12 h),[21] AMP−CaALG microcapsules (t_e = 24 h),[27] and AMP−PAN resin (t_e = 24 h).[28] To ensure adsorption equilibrium, a contact time of at least 24 h was utilized in the subsequent adsorption experiments.

The nonlinear equations of pseudo-first-order eq 5 and pseudo-second-order eq 5 models have been applied to describe the experimental data of Cs^+ adsorption kinetics

$$q_t = (1 - e^{-k_1 t}) \tag{5}$$

$$q_t = \frac{k_2 q_e^2 t}{(1 + k_2 q_e t)} \tag{6}$$

where k_1 (h^{-1}) and k_2 [g/(mg·h)] are the rate constants for pseudo-first-order and pseudo-second-order model, respectively, q_e (mg/g) is the equilibrium adsorption capacity, and q_t (m/g) is the adsorbed amount of Cs^+ at the instant time t (h). The fitting parameters are presented in Table 1. The pseudo-second-order model exhibited a better fit with the data compared to the pseudo-first-order model, as indicated by the relatively high correlation coefficient (R^2) values. This demonstrated that Cs^+ adsorption on the prepared beads occurred via chemical adsorption, which was attributed to the ion exchange between Cs^+ and NH_4^+ in the AMP lattice.

Table 1. Kinetic Parameters for the Adsorption of Cs^+ on ACS-1.0 Beads

pseudo-first-order-model			pseudo-second-order model		
k_1 (h^{-1})	q_e (mg/g)	R^2	k_2 (g/(g h))	q_e (mg/g)	R^2
0.26	5.31	0.85	0.063	5.32	0.96

3.3. HNO_3 Concentration Effect. HNO_3 was used to dissolve spent nuclear fuel to obtain the feed liquid for the next processing step. As a result, the actual HLLW contains a substantial amount of HNO_3 (2.0−5.0 mol/L),[29] which affected the performance of adsorbent in removing Cs^+. To elucidate the effect of HNO_3 concentration on the adsorption of Cs^+ onto the as-prepared beads, the uptake of Cs^+ at different initial concentrations (1.88 × 10^{-4} and 3.74 × 10^{-4}

https://doi.org/10.1021/acsomega.4c03806
ACS Omega 2024, 9, 32011−32020

mol/L) was studied under various HNO_3 concentrations. The K_d value was calculated to describe the affinity of the beads for Cs^+. As depicted in Figure 6, the K_d of Cs^+ exhibited a slight

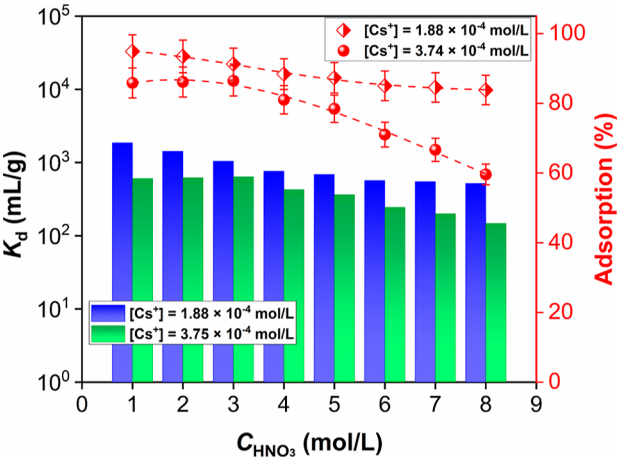

Figure 6. Effect of HNO_3 concentration on the adsorption of Cs^+ on ACS-1.0 beads. m/V = 10 g/L.

decrease as the concentration of HNO_3 increased from 1.0 to 8.0 mol/L. This can be attributed to the competing adsorption of H^+. Furthermore, the K_d values of Cs^+ at 1.88×10^{-4} mol/L were consistently higher than those of Cs^+ at 3.47×10^{-4} mol/L, indicating that Cs^+ removal efficiency decreased with the increase of Cs^+ concentration. Impressively, the ACS-1.0 beads demonstrated remarkable efficiency for different concentrations of Cs^+ over a wide range of HNO_3 concentrations from 1.0 to 3.0 mol/L, with adsorption percentage >86.5% and K_d values all above 6.3×10^2 mL/g. Even in 8.0 mol/L HNO_3 solution, the K_d value for Cs^+ at a concentration of 3.74×10^{-4} mol/L was still 1.6×10^2 mL/g (adsorption percentage = 59.4%). Several studies have reported similar results regarding the K_d values of Cs^+ for AMP-based composites under strongly acidic conditions. Park et al.[30] found that the K_d values of Cs^+ on the AMP/SBA-15 composite ranged from 10^3 to 10^2 mL/g in the presence of 0.01−2.5 mol/L HNO_3. Deng et al.[31] observed that the K_d value of Cs^+ on the AMP−silica matrix (SM) composite at 0.001−3.0 mol/L HNO_3 was approximately 775−800 mL/g. The excellent Cs^+ ion-exchange properties of ACS-1.0 beads in strongly acidic conditions emphasize its potential for removing Cs^+ from acidic waste streams.

3.4. Adsorption Isotherm. The exchange capacity of ACS-1.0 beads for Cs^+ in 3.0 mol/L HNO_3 solution have been measured by equilibrium isotherm studies, where initial concentrations of Cs^+ were varied from 1.1×10^{-4} to 8.8×10^{-3} mol/L. As depicted in Figure 7, the adsorption capacity increased significantly with increasing the initial Cs^+ concentration in the concentration range from 1.1×10^{-4} to 3.0×10^{-3} mol/L, which was due to the relatively sufficient reaction sites for Cs^+ adsorption. As the initial Cs^+ concentration continued to increase, the increasing trend of adsorption capacity was slowed.

The experimental data were simulated using the non-linear equations of both Langmuir model and Freundlich model to understand the adsorption mechanism.

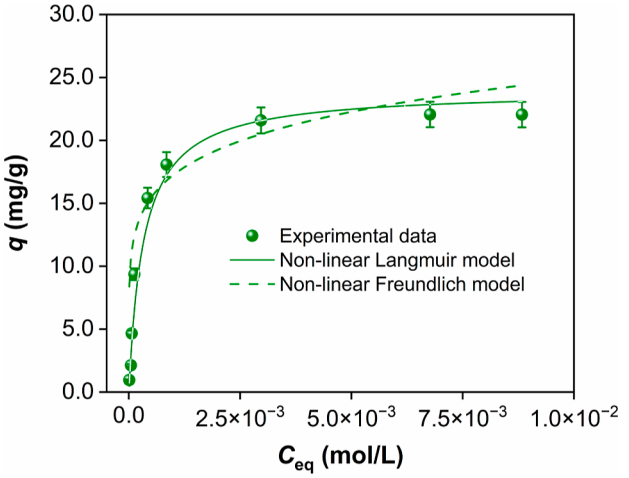

Figure 7. Experimental data and simulated curve for the adsorption isotherm of Cs^+ on ACS-1.0 beads. m/V = 10 g/L, [HNO_3] = 3.0 mol/L.

$$q = \frac{q_{max} \cdot K_L \cdot C_{eq}}{1 + K_L \cdot C_{eq}} \quad (7)$$

$$q = K_F \cdot C_{eq}^{1/n} \quad (8)$$

where q (mg/g) and C_{eq} (mol/L) are the concentrations of Cs^+ in the solid phase and the aqueous phase at adsorption equilibrium, respectively. q_{max} (mg/g) is the maximum exchange capacity and K_L (L/mol) is the Langmuir equation constant. K_F (mg/g)·(L/mol)$^{1/n}$ is the Freundlich constant, and the n is related to the free energy of adsorption. The related parameters of Cs^+ adsorption on ACS-1.0 beads are calculated from the two models, and the results are listed in Table 2. The higher correlation coefficient for the Langmuir

Table 2. Isotherm Model Parameters for the Adsorption of Cs^+ on ACS-1.0 Beads

Langmuir model			Freundlich model		
q_{max} (mg/g)	K_L (mg/g)	R^2	K_F (mg/g)·(L/mol)$^{1/n}$	n	R^2
23.9	3.01×10^3	0.93	51.62	6.30	0.84

model indicated that the Langmuir model was more suitable to describe the adsorption mechanism and the adsorption was a monolayer homogeneous adsorption process.[32] The maximum exchange capacity of ACS-1.0 beads for Cs^+ in strongly acidic solutions (3.0 mol/L HNO_3) was determined to be 23.9 mg/g. Table 3 presented the maximum exchange capacities of ACS-1.0 beads obtained in this study and reported other AMP-based composites under acidic conditions. It was found that the maximum exchange capacity of ACS-1.0 beads is in the middle of these adsorbents, indicating its potential for practical applications and the need for further research.

3.5. Selectivity in Simulated HLLW. Since there are more than 40 elements and 400 nuclides in HLLW,[38] the selectivity of Cs^+ capture has been considered as one of the most important factors in evaluating an adsorbent. Herein, we conducted a typical experiment with simulated HLLW containing eight competing cations and 3.0 mol/L HNO_3. The original concentration of metal ions in simulated HLLW as well as the adsorption percentage is summarized in Table 4.

https://doi.org/10.1021/acsomega.4c03806
ACS Omega 2024, 9, 32011−32020

Table 3. Comparisons between ACS-1.0 Beads and other AMP Composite Materials for Cs^+ Adsorption

materials	equilibrium time (h)	maximum exchange capacity (mg/g)	HNO_3 (mol/L)	references
pure AMP	1.5	91.5	0.01	33
AMP/SiO_2	12	20.56	3.0	9
SM−AMP20	4.0	37.6	0.001−3.0	31
AMP−Al_2O_3	∼1	12.0	2.0	34
AMP/zirconium phosphate	7	6.0	2.0	35
AMP−PAN	2.5	41.2	4.0	36
AMP−PMMA	24	25.1−32.7	0.1−5.0	37
AMP−CaALG−silica	12	23.9	3.0	this work

Table 4. Adsorption Percentage of Cs^+ as well as the Other Metal Ions in Simulated HLLW

metal ions	original concentration (mol/L)	adsorption percentage (%)
Cs^+	3.75×10^{-4}	89.8
Al^{3+}	1.03×10^{-2}	2.5
Cr^{3+}	6.37×10^{-4}	0.1
Fe^{3+}	6.18×10^{-3}	0.3
K^+	2.03×10^{-4}	0.9
Na^+	3.83×10^{-3}	1.8
Nd^{3+}	4.07×10^{-4}	2.3
Ni^{2+}	3.07×10^{-3}	1.4
Sr^{2+}	1.47×10^{-4}	5.7

A significantly higher value of 89.3% for Cs^+ was obtained compared to other metal ions present in the solution, even with higher concentrations (Al^{3+}, Fe^{3+}, Na^+, Nd^{3+}, and Ni^{2+}). As the metal ions had different initial concentration, more intuitive comparisons of K_d value and separation factor SF are shown in Figure 8a,b, respectively. The results demonstrated that the ACS-1.0 beads had dominant selectivity toward Cs^+, as evidenced by a K_d value of 886 mL/g and SF values all above 145. Among the miscellaneous interferences, only the Sr^{2+} showed a certain extent of affinity to the adsorbent (adsorption percentage = 5.7%), indicating that Sr^{2+} poses the most robust competition with Cs^+ among the simulated HLLW. However, a remarkable $SF_{Cs/Sr}$ of ∼145 indicates that the competitive effect of Sr^{2+} on the adsorption of Cs^+ would not be a significant problem in practical applications. Typically, the two ions can be well separated when the SF value is higher than 100.[39]

3.6. XPS Characterization. The excellent adsorption ability and high selectivity of the ACS-1.0 beads for Cs^+ were observed in the present work, which can be attributed to the ion exchange mechanism of AMP as an inorganic ion exchanger on the composite. Figure 9 shows the results of XPS characterization of the beads before and after adsorption of Cs^+. After Cs^+ adsorption, the peaks of Cs $3d^3$ and Cs $3d^5$ could be observed at the binding energies of 738.7 and 724.2 eV, and the intensity of the N 1s peak and Mo 3d peak on the adsorbent was obviously decreased. These results experimentally indicated the ion exchange process between Cs^+ and NH_4^+ in the beads. Similar observations have been reported in the uptake of Cs^+ by silica-based AMP adsorbent (AMP/

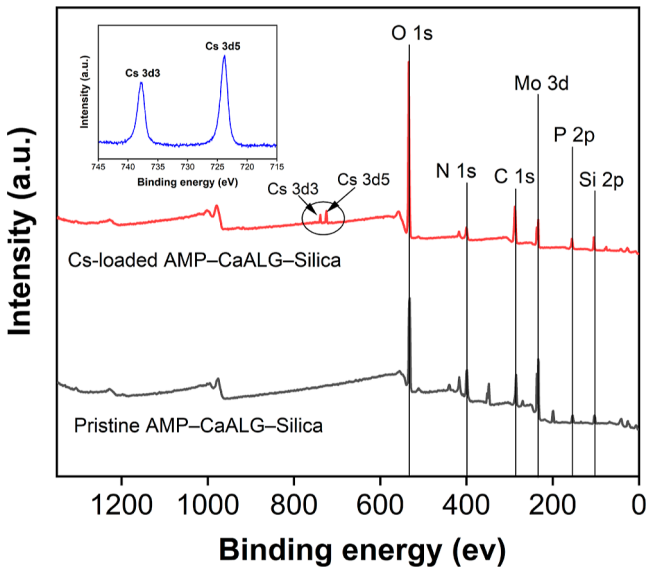

Figure 9. XPS survey spectra of ACS-1.0 beads before and after Cs^+ adsorption.

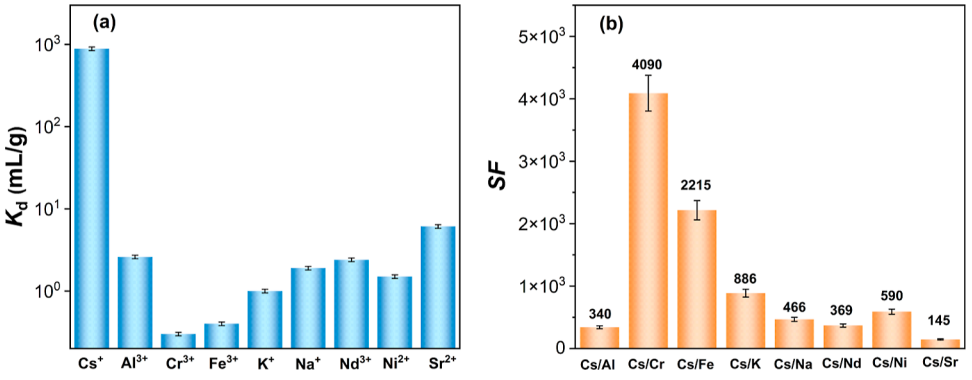

Figure 8. K_d value of metal ions (a) and the separation factor SF of Cs^+ from interfering metals (b) in simulated HLLW. m/V = 10 g/L, [HNO_3] = 3.0 mol/L.

https://doi.org/10.1021/acsomega.4c03806
ACS Omega 2024, 9, 32011−32020

SiO_2).[9] The hydrated ionic radius of Cs^+ (3.29 Å) and NH_4^+ (3.31 Å) are similar, leading to a preference for ion exchange of Cs^+ with NH_4^+ in the cavities of the AMP crystal compared to other monovalent ions. This is also consistent with the values of the Gibbs free energy for cation exchange in AMP,[40] where AMP material showed the highest affinity for Cs^+.

3.7. Desorption Performance. NH_4^+ could exchange with the Cs^+ adsorbed on the ACS-1.0 composite to achieve desorption of Cs^+. Thus, the Cs^+ containing composite could be desorbed using NH_4NO_3 in the present work. As depicted in Figure 10, the desorption efficiency was increased with the

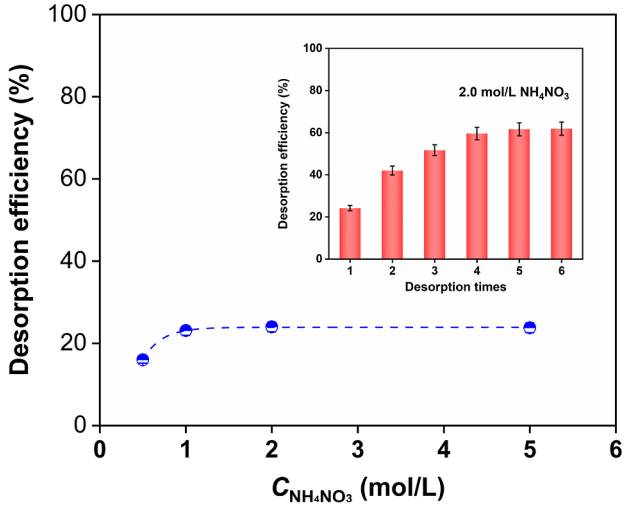

Figure 10. Effect of NH_4NO_3 concentration and desorption times on the desorption efficiency of ACS-1.0 beads. $[Cs^+] = 3.75 \times 10^{-4}$ mol/L, m/V = 10 g/L, and $[HNO_3]$ = 3.0 mol/L.

NH_4NO_3 concentration when it was below 1.0 mol/L, whereas negligible increase was observed within the NH_4NO_3 concentration range of 1.0−6.0 mol/L. The desorption efficiency was found to be approximately 24% after the initial desorption treatment using 2.0 mol/L NH_4NO_3, and the desorption efficiency was only up to 61% after six cycles. These results indicate that the ACS-1.0 beads possessed poor desorption properties for Cs^+. However, it also demonstrates the strong binding of Cs^+ by the binding sites of the adsorbent. This is in particular advantageous when the ACS-1.0 beads is to be used for safe immobilization of radioactive Cs^+. The immobilization of radioactive Cs^+ waste in stable materials is a globally acknowledged approach to prevent its migration into the biosphere and potential harm to human health during storage. A pressing/sintering method using natural additives like allophane or a combination of allophane and zeolite has been suggested for the stable solidification of the used adsorbent.[41]

3.8. Column Experiment. The removal of Cs^+ from simulated HLLW was investigated using an ACS-1.0 beads packed column to evaluate the potential of the beads for practical applications. In order to achieve an earlier breakthrough, the concentration of all metal ions in the simulated HLLW (as shown in Table 2) was uniformly increased by 10.0 times. As depicted in Figure 11, the breakthrough curve of Cs^+ displayed a characteristic S-shape, indicating a notable dynamic adsorption rate and efficient utilization of the column. Usually, the 5% breakthrough point is used as a momentous indicator to evaluate the adsorption performance of the adsorbent in

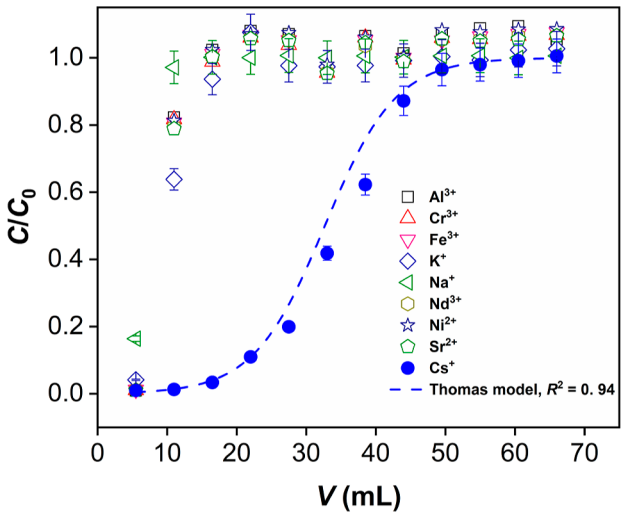

Figure 11. Breakthrough curves involving in simulated HLLW. $[HNO_3]$ = 3.0 mol/L.

industrial applications.[42] The 5% breakthrough volume and the capacity of maximum dynamic exchange capacity can be estimated by the Thomas model.

$$\frac{C}{C_0} = \frac{1}{\exp\left(\frac{K_T \cdot Q_{max} \cdot m}{v} - \frac{K_T \cdot C_0 \cdot V}{v}\right)} \quad (9)$$

where C and C_0 (mol/L) were concentrations of Cs^+ in the effluents and influents, respectively; K_T (mL/min/mol) is the rate constant in the Thomas model; Q_{max} (mol/g) the maximum exchange capacity of the adsorbent in the exchange column; m (g) the mass of adsorbent; V (mL) the volume of effluent; and v (mL/min) is the flow rate of solution.

According to the Thomas model, the 5% breakthrough volume of Cs^+ in the simulated HLLW containing 3.0 mol/L HNO_3 was approximately 18.0 mL, and the maximum dynamic exchange capacity was estimated to be 15.6 mg/g, which is lower than the adsorption capacity obtained using the batch method (23.9 mg/g). Under this working condition, the Cs^+ (3.75×10^{-3} mol/L) in the simulated HLLW was completely adsorbed before 5 adsorption bed volumes. As for the other coexisting ions, the breakthrough occurred rapidly after the simulated HLLW occupied the dead volume, which was approximately 11 mL. Notably, hitherto studies on the column removal of Cs^+ from the HLLW containing highly concentrated HNO_3 using AMP-based composites are still rare.[9,27] The above results demonstrate that the ACS-1.0 beads have significant potential as a column packing material for effectively removing Cs^+ from the HLLW.

4. CONCLUSIONS

In the present work, a novel millimeter-sized AMP-based material, ACS beads, was prepared by encapsulating the fine crystals of the AMP exchanger into a calcium alginate−SM. The mass ratio of AMP to silica in the composite was optimized, and the experiment results indicated that ACS beads with an AMP/silica mass ratio of 1.0 exhibited relatively excellent mechanical strength, along with good adsorption capacity (q_{max} = 23.9 mg/g) and selectivity (SF > 145) toward Cs^+ in HNO_3 solutions and the simulated HLLW. In addition, the dynamic column experiment exhibited that the beads were effective for the selective remove Cs^+ from strongly acidic

https://doi.org/10.1021/acsomega.4c03806
ACS Omega 2024, 9, 32011−32020

simulated HLLW. The main findings of this study highlight the successful fabrication of new and low-cost ACS beads with excellent physical-chemical properties, making them promising candidates for industrial applications. The Cs^+ adsorption kinetics, isotherm, and selectivity results presented in the paper provide valuable insights into the potential of these beads for efficient radiocesium removal.

AUTHOR INFORMATION

Corresponding Author

Zhijun Guo − *MOE Frontiers Science Center for Rare Isotopes, Lanzhou University, Lanzhou 730000, China; Radiochemistry Laboratory, School of Nuclear Science and Technology and The Key Laboratory of Special Function Materials and Structure Design, Ministry of Education, Lanzhou University, Lanzhou 730000, China;* orcid.org/0000-0002-2371-8854; Email: guozhj@lzu.edu.cn

Authors

Qiang Jin − *MOE Frontiers Science Center for Rare Isotopes, Lanzhou University, Lanzhou 730000, China; Radiochemistry Laboratory, School of Nuclear Science and Technology and The Key Laboratory of Special Function Materials and Structure Design, Ministry of Education, Lanzhou University, Lanzhou 730000, China;* orcid.org/0009-0004-1631-9312

Xinya Diao − *MOE Frontiers Science Center for Rare Isotopes, Lanzhou University, Lanzhou 730000, China; Radiochemistry Laboratory, School of Nuclear Science and Technology, Lanzhou University, Lanzhou 730000, China*

Ye Fan − *MOE Frontiers Science Center for Rare Isotopes, Lanzhou University, Lanzhou 730000, China; Radiochemistry Laboratory, School of Nuclear Science and Technology, Lanzhou University, Lanzhou 730000, China*

Lecun Hao − *MOE Frontiers Science Center for Rare Isotopes, Lanzhou University, Lanzhou 730000, China; Radiochemistry Laboratory, School of Nuclear Science and Technology, Lanzhou University, Lanzhou 730000, China*

Zongyuan Chen − *MOE Frontiers Science Center for Rare Isotopes, Lanzhou University, Lanzhou 730000, China; Radiochemistry Laboratory, School of Nuclear Science and Technology and The Key Laboratory of Special Function Materials and Structure Design, Ministry of Education, Lanzhou University, Lanzhou 730000, China*

Complete contact information is available at: https://pubs.acs.org/10.1021/acsomega.4c03806

Notes

The authors declare no competing financial interest.

ACKNOWLEDGMENTS

This work was funded by the Natural Science Foundation of Gansu Province, China (nos 21ZD8JA006 and 22JR5RA480), the National Natural Science Foundation of China (no. 12175094), and the Fundamental Research Funds for the Central Universities (lzujbky-2023-stlt01, lzujbky-2022-sp05, and lzujbky-2022-kb01).

REFERENCES

(1) Ewing, R. C. Long-term storage of spent nuclear fuel. *Nat. Mater.* **2015**, *14*, 252−257.

(2) Yoshikawa, H.; Sunada, S.; Hirakawa, H.; Fujimori, A.; Elmegerhi, S.; Leary, D.; Kato, T. A. Radiobiological characterization of canine malignant melanoma cell lines with different types of ionizing radiation and efficacy evaluation with cytotoxic agents. *Int. J. Mol. Sci.* **2019**, *20*, 841.

(3) Artun, O. A study of nuclear structure for ^{244}Cm, ^{241}Am, ^{238}Pu, ^{210}Po, ^{147}Pm, ^{137}Cs, ^{90}Sr and ^{63}Ni nuclei used in nuclear battery. *Mod. Phys. Lett.* **2017**, *32*, 1750117.

(4) Tosri, C.; Chusreeaeom, K.; Limtiyayotin, M.; Sukin, N.; Jompuk, P. Comparative effect of high energy electron beam and ^{137}Cs gamma ray on survival, growth and chlorophyll content in curcuma hybrid 'laddawan' and determine proper dose for mutations breeding. *Emir. J. Food. Agr.* **2019**, *31*, 321−327.

(5) Wang, J. L.; Zhang, S. Removal of cesium ions from aqueous solutions using various separation technologies. *Rev. Environ. Sci. Bio/Technol.* **2019**, *18*, 231−269.

(6) Rahman, R. O. A.; Ibrahium, H. A.; Hung, Y. T. Liquid radioactive wastes treatment: a review. *Water* **2011**, *3*, 551−565.

(7) Chen, S. Q.; Hu, J. Y.; Han, S. J.; Guo, Y. F.; Belzile, N.; Deng, T. L. A review on emerging composite materials for cesium adsorption and environmental remediation on the latest decade. *Sep. Purif. Technol.* **2020**, *251*, 117340.

(8) Smit, J. V. R. Ammonium salts of the heteropolyacids as cation exchangers. *Nature* **1958**, *181*, 1530−1531.

(9) Sang, H. J.; Mao, C.; Ming, F. C.; Xu, L. J.; Wei, Y. Z.; Wu, Y. Selective separation and immobilization process of ^{137}Cs from high-level liquid waste based on silicon-based heteropoly salt and natural minerals. *Chem. Eng. J.* **2022**, *449*, 137842.

(10) Alby, D.; Charnay, C.; Heran, M.; Prelot, B.; Zajac, J. Recent developments in nanostructured inorganic materials for sorption of cesium and strontium: synthesis and shaping, sorption capacity, mechanisms, and selectivity—a review. *J. Hazard. Mater.* **2018**, *344*, 511−530.

(11) Sutirman, Z. A.; Sanagi, M. M.; Aini, W. I. W. Alginate-based adsorbents for removal of metal ions and radionuclides from aqueous solutions: a review. *Int. J. Biol. Macromol.* **2021**, *174*, 216−228.

(12) Wang, J. L.; Chen, C. Biosorbents for heavy metals removal and their future. *Biotechnol. Adv.* **2009**, *27*, 195−226.

(13) Zhang, S.; Xu, F.; Zhang, W. Z.; Peng, X. I.; Pepe, F.; Pepe, F. Silica modified calcium alginate-xanthan gum hybrid bead composites for the removal and recovery of Pb(II) from aqueous solution. *Chem. Eng. J.* **2013**, *234*, 33−42.

(14) Sánchez-Téllez, D. A.; TéLlez-Jurado, L.; RodrÍGuez-Lorenzo, L. Hydrogels for cartilage regeneration, from polysaccharides to hybrids. *Polymers* **2017**, *9*, 671.

(15) Boninsegna, S.; Toso, R. D.; Monte, R. D.; Carturan, G. Alginate microspheres loaded with animal cells and coated by a siliceous layer. *J. Sol-Gel Sci. Technol.* **2003**, *26*, 1151−1157.

(16) Coradin, T.; Mercey, E.; Lisnard, L.; Livage, J. Design of silica-coated microcapsules for bioencapsulation. *Chem. Commun.* **2001**, 2496−2497.

(17) Coradin, T.; Nassif, N.; Livage, J. Silica-alginate composites for microencapsulation. *Appl. Microbiol. Biotechnol.* **2003**, *61*, 429−434.

(18) Hernández-González, A. C.; Téllez-Jurado, L.; RodrÍGuez-Lorenzo, L. M. Preparation of covalently bonded silica-alginate hybrid hydrogels by SCHIFF base and sol-gel reactions. *Carbohydr. Polym.* **2021**, *267*, 118186.

(19) Annenkov, V. V.; Danilovtseva, E. N.; Pal'shin, V. A.; Verkhozina, O. N.; Zelinskiy, S. N.; Krishnan, U. M. Silicic acid condensation under the influence of water-soluble polymers: from biology to new materials. *RSC Adv.* **2017**, *7*, 20995−21027.

(20) Burneau, A.; Humbert, B.; BarrÈS, O.; Gallas, J. P.; Lavalley, J. C. Fourier transform infrared and Raman spectroscopic study of silica surfaces. *Adv. Biochem.* **1994**, *234*, 200−222.

(21) Chen, S. Q.; Hu, J. Y.; Shi, J.; Wang, M. X.; Guo, Y. F.; Li, M. L.; Duo, J.; Deng, T. L. Composite hydrogel particles encapsulated ammonium molybdophosphate for efficiently cesium selective removal and enrichment from wastewater. *J. Hazard. Mater.* **2019**, *371*, 694−704.

(22) Yang, H. J.; Yu, H. W.; Sun, J. K.; Liu, J. T.; Xia, J. B.; Fang, J. D.; Li, Y.; Qu, F. Z.; Song, A. Y.; Wu, T. Facile synthesis of

mesoporous magnetic AMP polyhedric composites for rapid and highly efficient separation of Cs^+ from water. *Chem. Eng. J.* **2017**, *317*, 533−543.
(23) Larosa, C.; Salerno, M.; Lima, J. S. D.; Meri, R. M.; Silva, M. F. D.; Carvalho, L. B. D.; Converti, A. Characterisation of bare and tannase-loaded calcium alginate beads by microscopic, thermogravimetric, FTIR and XRD analyses. *Int. J. Biol. Macromol.* **2018**, *115*, 900−906.
(24) Biswas, R. K.; Khan, P.; Mukherjee, S.; Mukhopadhyay, A. K.; Ghosh, J.; Muraleedharan, K. Study of short range structure of amorphous silica from pdf using ag radiation in laboratory XRD system, RAMAN and NEXAFS. *J. Non-Cryst. Solids* **2018**, *488*, 1−9.
(25) Dermeche, L.; Thouvenot, R.; Hocine, S.; Rabia, C. Preparation and characterization of mixed ammonium salts of keggin phosphomolybdate. *Inorg. Chim. Acta* **2009**, *362*, 3896−3900.
(26) Thommes, M.; Kaneko, K.; Neimark, A. V.; Olivier, J. P.; Rodriguez-Reinoso, F.; Rouquerol, J.; Sing, K. S. W. Physisorption of gases, with special reference to the evaluation of surface area and pore size distribution (IUPAC Technical Report). *Pure Appl. Chem.* **2015**, *87*, 1051−1069.
(27) Mimura, H.; Saito, M.; Akiba, K.; Onodera, Y. Selective uptake of cesium by ammonium molybdophosphate (AMP)-calcium alginate composites. *J. Nucl. Sci. Technol.* **2001**, *38*, 872−878.
(28) Yang, J. Q.; Wang, M.; Zhang, L. L.; Lu, Y. M.; Di, B.; Shi, K. L.; Hou, X. L. Investigation on the thermal stability of cesium in soil pretreatment and its separation using AMP-PAN resin. *J. Radioanal. Nucl. Chem.* **2023**, *332*, 877−885.
(29) Ning, S. Y.; Wang, X. P.; Zou, Q.; Shi, W. Q.; Tang, F. D.; He, L. F.; Wei, Y. Z. Direct separation of minor actinides from high level liquid waste by Me_2-CA-BTP/SiO_2-P adsorbent. *Sci. Rep.* **2017**, *7*, 14679.
(30) Pack, Y.; Shin, W. S.; Choi, S. J. Ammonium salt of heteropoly acid immobilized on mesoporous silica (SBA-15): an efficient ion exchanger for cesium ion. *Chem. Eng. J.* **2013**, *220*, 204−213.
(31) Deng, H.; Li, Y. X.; Huang, Y.; Ma, X.; Wu, L.; Cheng, T. H. An efficient composite ion exchanger of silica matrix impregnated with ammonium molybdophosphate for cesium uptake from aqueous solution. *Chem. Eng. J.* **2016**, *286*, 25−35.
(32) Wang, Y. P.; Li, K. X.; Fang, D. Z.; Ye, X. S.; Liu, H. N.; Tan, X. L.; Li, Q.; Li, J.; Wu, Z. J. Ammonium molybdophosphate/metal-organic framework composite as an effective adsorbent for capture of Rb^+ and Cs^+ from aqueous solution. *J. Solid State Chem.* **2022**, *306*, 122767.
(33) Yi, T. Z.; Ya, H. Z.; Dong, Z.; Lin, W. X. Structural characterization of ammonium molybdophosphate with different amount of cesium adsorption. *J. Radioanal. Nucl. Chem.* **2014**, *299*, 1165−1169.
(34) Chakravarty, R.; Ram, R.; Pilla, K. T.; Pamale, Y.; Kamat, R. V.; Dash, A. Ammonium molybdophosphate impregnated alumina microspheres as a new generation sorbent for chromatographic $^{137}Cs/^{137m}Ba$ generator. *J. Chromatogr. A* **2012**, *1220*, 82−91.
(35) Murthy, G. S.; Sivaiah, M. V.; Kumar, S. S.; Reddy, V. N.; Krishna, R. M.; Lakshminarayana, S. Adsorption of cesium on a composite inorganic exchanger zirconium phosphate-ammonium molybdophosphate. *J. Radioanal. Nucl. Chem.* **2004**, *260*, 109−114.
(36) Mahendra, C.; Sathya, P. M. S.; Babu, C. A.; Revathy, K.; Rajan, K. K. Analysis and modeling of fixed bed sorption of cesium by AMP-PAN. *J. Environ. Chem. Eng.* **2015**, *3*, 1546−1554.
(37) Banerjee, D.; Rao, M. A.; Gabriel, J.; Samanta, S. K. Recovery of purified radiocesium from acidic solution using ammonium molybdophosphate and resorcinol formaldehyde polycondensate resin. *Desalination* **2008**, *232*, 172−180.
(38) Koyama, S.; Suzuki, T.; Ozawa, M. From waste to resource, nuclear rare metals as a dream of modern alchemists. *Energy Convers. Manage.* **2010**, *51*, 1799−1805.
(39) Mertz, J. L.; Fard, Z. H.; Malliakas, C. D.; Manos, M. J.; Kanatzidis, M. J. Selective removal of Cs^+, Sr^{2+}, and Ni^{2+} by K_{2x} mg_x $sn_{3-X}s_6$ (X = 0.5−1) (KMS-2) relevant to nuclear waste remediation. *Chem. Mater.* **2013**, *25*, 2116−2127.
(40) Solange, S. *Molybdophosphate d'ammonium immobilisé sur silice mésoporeuse pour l'adsorption sélective du radiocésium*; Laval University, 2012.
(41) Cheng, Y.; Wang, Y. Q.; Sang, H. J.; Wu, Y.; Wei, Y. Z. Study on the immobilization of cesium absorbed by copper ferrocyanide using allophane through pressing/sintering method. *J. Nucl. Mater.* **2020**, *532*, 152008.
(42) Tang, J. H.; Jin, J. C.; Li, W. A.; Zeng, X.; Ma, W.; Li, J. L.; Lv, T. T.; Peng, Y. C.; Feng, M. L.; Huang, X. Y. Highly selective cesium(I) capture under acidic conditions by a layered sulfide. *Nat. Commun.* **2022**, *13*, 658.

https://doi.org/10.1021/acsomega.4c03806
ACS Omega 2024, 9, 32011−32020